Major axis steel joint under torsion
Stiffness and strength characterization

Gil, Beatriz; Goñi, Rufino; Bijlaard, Frans; Bayo, Eduardo

DOI
10.1016/j.engstruct.2018.11.060

Publication date
2019

Document Version
Accepted author manuscript

Published in
Engineering Structures

Major axis steel joint under torsion: Stiffness and strength characterization.

Beatriz Gil [a], Rufino Goñi [b], Frans Bijlaard [c], Eduardo Bayo [d]

[a b d] *University of Navarra. Department of Construction, Services and Structures*

31080 Pamplona, Spain.

[c] *Delft University of Technology.*

Corresponding author. Email: bgilr@unav.es

Abstract

Torsional effects in joints need to be investigated in order to get a complete model of the joint and also to assess the real boundary conditions for the lateral torsional effects in the beams of structural frames. Phenomena such as: torsion, warping, lateral buckling, etc. are usually analysed assuming simplified boundary conditions, namely pinned or rigid, in frame analysis which can lead to erroneous and non-conservative results.

With the aim of knowing the correct boundary conditions and real behaviour of the joints under torsion, an experimental program is carried out consisting of two tests of mayor axis doubled extended bolted end plate joints subjected to torsion about the axis along the length of the beam. These experimental results have allowed the validation of the finite element models carried out using the program Abaqus. Once the models are validated models, a parametric study is performed to assess the stiffness and resistance. This study also verifies that these joints behave in a semi-rigid way when compared with the torsional characteristics of the attached beam. Besides, the beam fails prior to the connection in most cases, and therefore, the joints can be assumed to behave as full-strength.

Analytical expressions are proposed and checked with the FEM results proving that the proposed analytical formulae and the proposed mechanical model can predict the stiffness quite accurately, with an average error of 8.5%. Despite these joints can be classified as full-strength under torsion, an assessment of their resistance is done as well.

Keywords

Steel joints, T-stub, torsion, warping, experimental, FEM, analytical characterization, component method

Notation list

B	Bimoment associated to the first derivative of rotation
b_b	Breath of the beam section
b_c	Breath of the column section
E	Young modulus
e_{ep}	Distance between the bolt and the end plate edge, measured horizontally
e_x	Distance between the bolt and the end plate edge, measured vertically.
F_B	Forces in which the torque T_B is subdivided
$F_{cf,t,Rd}$	Strength of the column flange in torsion
$F_{cw,b,Rd}$	Strength of the column web in bending
f_{yd}	Yield strength of structural steel
g	Distance between bolts axis, measured horizontally
G	Shear modulus
h_b	Beam height
I_{cw}	Inertia of the effective section of the column web
I_w	Warping constant
I_z	Minor axis moment of inertia
J	Torsional modulus of the considered section
$k_{cf,T}$	Translational stiffness coefficient for the column flange in torsion
$k_{cw,b}$	Stiffness coefficient for the column web in bending
$k_{1cf,t}$	Rotational stiffness coefficient of the column flange
$k_{2cf,t}$	Rotational stiffness coefficient of the column flange and end plate
L	Length of the beam or other element
L_c	Length of the column
$l_{eff,cw,b}$	Effective length of the column web in bending
$M_{pl,cw,Rd}$	Plastic resistant moment of the effective section of the column web
M_w	Warping moment in each T-stub of the joint
m_x	Distance between the bolts and the beam flange, measured vertically.
p	Pitch of the bolts

S_{ax} Translational stiffness

$S_{b,f}$ Beam flange or T-Stub bending stiffness

$S_{b,w}$ Warping stiffness of the beam

$S_{j,ax}$ Stiffness of the translational springs in each beam flange edge

$S_{j,f}$ Stiffness of the rotational spring for each beam flange or T-stub

$S_{j,w}$ Warping stiffness of the complete joint, for to the degree of freedom associated to the first derivative of rotation.

S_{rot} Rotational stiffness

t Thickness of the considered section

T_B Applied torque in the beam

T_c Torsional moment in the column flange

t_{fb} Thickness of beam flange

t_{fc} Column flange thickness

t_{ep} End plate thickness

$T_{pl,Rd}$ Plastic resistance of a rectangular section in torsion

t_{wc} Column web thickness

$W_{T,pl}$ Plastic torsional modulus

z Lever arm, distance between the bolts in tension and the resultant of compression for each T-Stub

θ Torsional rotation of the column flange in the zone of the joint

τ_y Maximum tangential stress is $\tau_y = \frac{f_{yd}}{\sqrt{3}}$

1. Introduction and objectives

Semi-rigid and partial strength steel connections have been dealt with for quite a few years. The research has been mainly focused on 2D joints, as well as in-plane behaviour and mayor axis loading [1]. A considerable amount of research has been dedicated to the behaviour of isolated components of the joints [2, 3]. 3D joints have been researched to a lesser extent. However, there are recent studies that have focused on the characterization of 3D joints [4-8], the out of plane behaviour [9, 10] and on minor axis connections [11].

Torsional effects in joints need to be investigated not only to get a complete model of the joint, but also to assess the real boundary conditions to the lateral torsional effects in the beams of structural frames. Reference [12] explores a range of situations where torsion may appear in beams of portal frames. Phenomena such as: torsion, warping, lateral buckling, etc. are usually analysed assuming simplified boundary conditions, such as pinned or rigid, in frame analysis, which can lead to erroneous and non-conservative results. Modern codes, including Eurocode 3 [13], allow the stability checks to be done by advanced formulations that require a correct assessment of the stiffness and strength properties of the joints and element boundary conditions.

With the aim to obtain knowledge of the correct boundary conditions and behaviour of the joints under torsion, an experimental program is carried out consisting of two tests of mayor axis doubled extended bolted end plate joints subjected to torsion about the length axis of the beam. The tested joints do not have either stiffeners or additional plates. The experimental results show that the joints can be considered as rigid for St Venant torsion, but should be considered semi-rigid under warping. At the same time, these experimental results have allowed the validation of the finite element models carried out using the program ABAQUS [14].

With the validated finite element models, a parametric study is carried out varying the beam and column sizes, the bolt diameters, the end plate thicknesses and the distances between bolts and edges.

Analytical expressions for the stiffness are proposed and checked with the FEM results proving that the proposed analytical formulae and mechanical model can predict the stiffness quite accurately. However and in regard to the resistance, finite element simulations could not provide any results since the beams failed before the connection in practically all cases, thus corroborating that the joint can be classified as full-strength. Nevertheless, an analytical assessment of the resistance is made in Section 4 based on the component method.

2. Experimental program

The experimental program focussed on the testing of two specimens with doubled extended end plate steel joints subjected to torsion. The two specimens are composed of an IPE beam attached to a HEA column in its major axis through a symmetrical extended end plate with four bolts in both the upper and lower flange area. The column does not have either plates or stiffeners. The specimens are lying horizontally and the column is clamped to a rigid frame as shown in Fig. 1.

The torque is applied by adding an arm (HEB section) to the far end of the beam. The arm is simply supported by a cylinder that allows the rotation but prevents the vertical displacement. The load is applied through a hydraulic jack, with a loading capacity of 400 kN, on the other side of the arm causing the torque in the beam which transmits it to the joint (see Fig. 1).

The far end of the beam is welded to the arm only in the web; and there is a fillet in the flanges in order to allow warping. Fig. 2 shows the configuration of the joint, and Table 1 summarizes the main characteristics of the two specimens. The differences between TT01 and TT02 are the column section, the beam section, the end plate thickness and the diameter of the bolts.

The sizes of the sections have been chosen in order to be realistic and consistent with the dimensions and loading conditions normally used in the structural design of buildings.

Table 1: Tested specimens

EXPERIMENTAL PROGRAM							
Test	**Column**	**Beam**	**Type**	**End plate**	**Additional plate**	**Steel**	**Joint**
TT01	HEA 160	IPE 300	Mayor axis	10 mm	No	S275	8 bolts ∅ 16(10.9)
TT02	HEA 140	IPE 270	Mayor axis	8 mm	No	S275	8 bolts ∅ 12(10.9)

2.1. Mechanical properties of the materials

The materials used in the specimens are: steel grade S275 for sections and plates, and class 10.9 for the bolts. Tensile coupons have been extracted from every kind of section and the end plates and have been tested to determine the real mechanical properties of the steel, according to the European standard [15]. These properties are shown in Table 2.

The true stress-strain curves are used to calibrate the finite element models with the experimental results. One example of the results coming from a coupon test is shown in Fig. 3. The remaining ones are very similar.

The bolts are class 10.9 and not preloaded. They are used instead of class 8.8 due to their higher resistance. The bolts are not key *components* in this research and have been over dimensioned to avoid their failure under tension and/or shear. Due to this fact strain gages have not been placed inside the bolts.

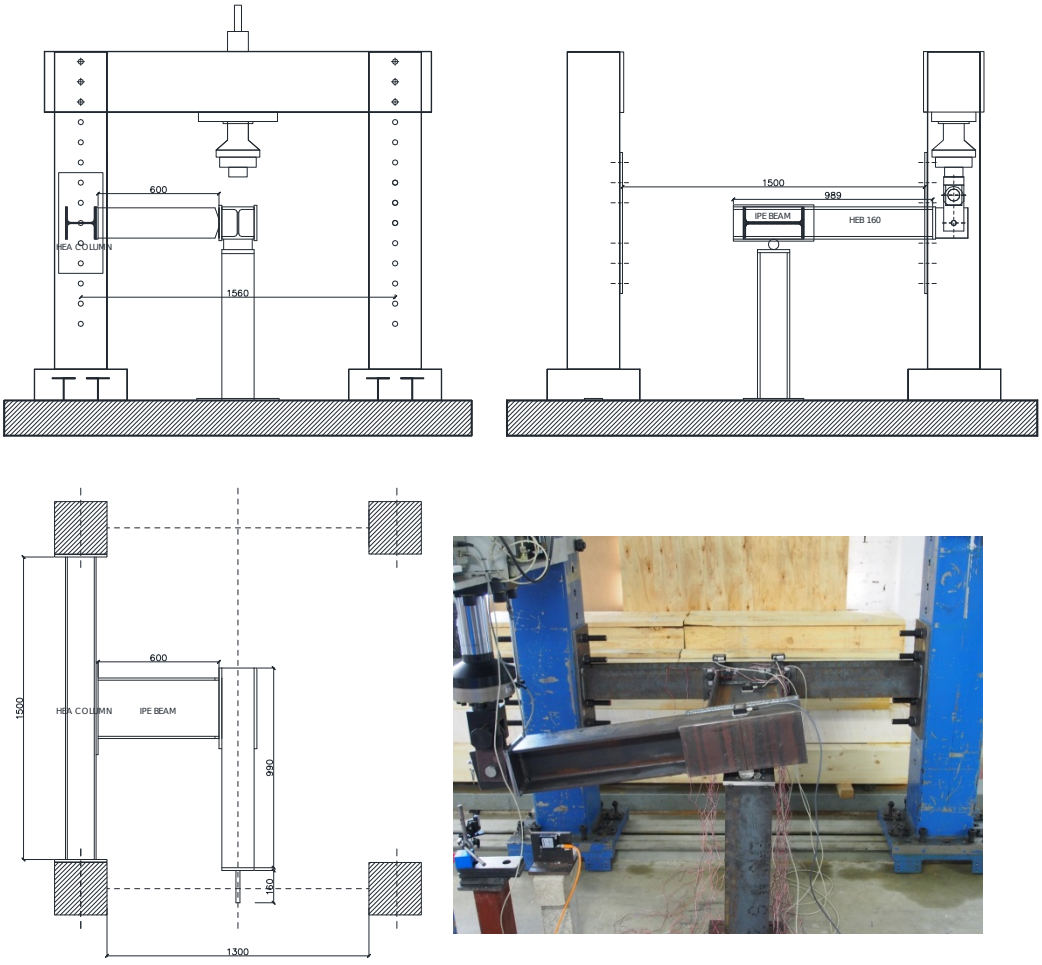

Fig.1: Test setup

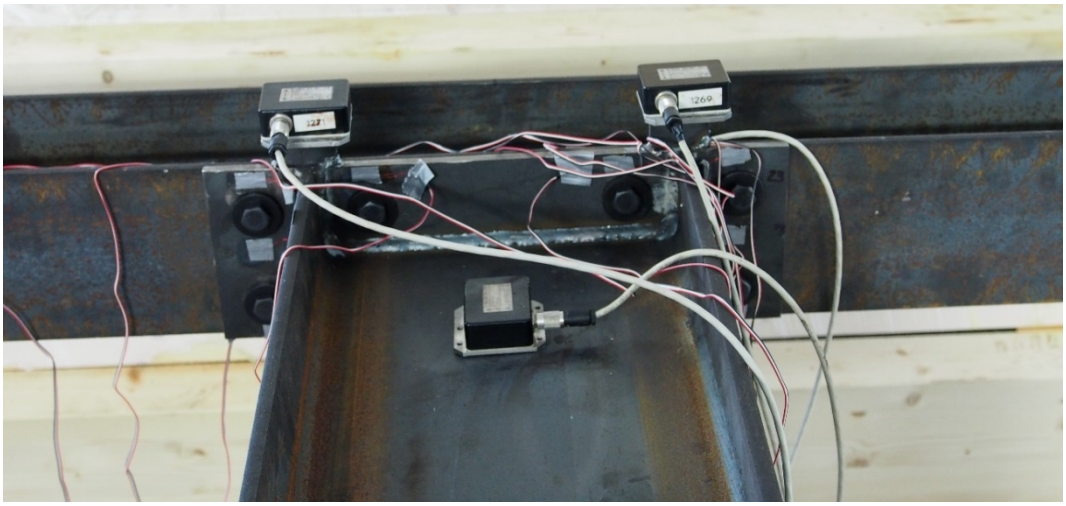

Fig. 2: Joint configuration for specimens TT01 and TT02

Table 2. Material properties: results of tensile coupon tests.

Material	Steel grade	Yield stress (MPa)	Young´s Modulus (MPa)	Tensile Strength (MPa)	% of elongation at fracture
TT02: End plate 8 mm	S275	328	210 200	460	37
TT01: End plate 10 mm	S275	332	222 600	461	36
TT02: IPE 270 Flange _A	S275	331	222 300	495	32.5
TT02: IPE 270 Flange _B	S275	336	220 800	499	32.0
TT02: IPE 270 Web	S275	355	204 300	503	34.0
TT01: IPE 300 Flange _A	S275	313	227 400	460	32.5
TT01: IPE 300 Flange _B	S275	312	208 800	456	30.0
TT01: IPE 300 Web	S275	339	212 300	467	37.0
TT02: HEA 140 Web A	S275	340	197 400	477	33.5
TT02: HEA 140 Web B	S275	335	213 000	477	38.0
TT01: HEA 160 Web A	S275	344	211 200	480	37.5
TT01: HEA 160 Web B	S275	345	214 000	484	37.5

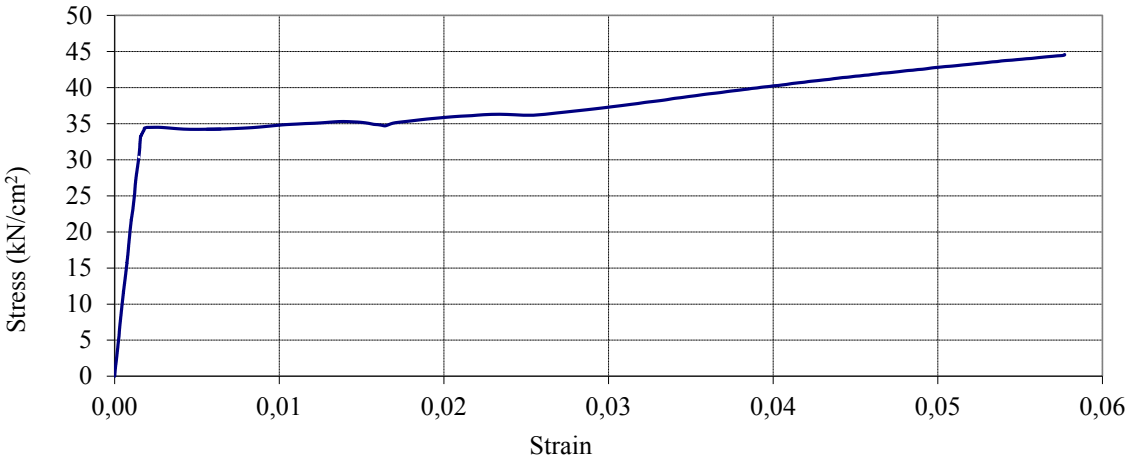

Fig. 3: True Stress vs. Strain curve for one coupon tests (HEA 160 web A).

2.2. Instrumentation and loading procedure

The most relevant sources of deformation are monitored through strain gauges that send the information to a Vishay data acquisition system. Rotations are measured by means of inclinometers. Fig. 4 shows the location of both the strain gauges and inclinometers. There are strain gauges on the right side of the end plate (ep.R1, ep.R2, ep.R3, ep.R4 and ep.R5), on the left side of the end plate (ep.L1, ep.L2, ep.L3, ep.L4 and ep.L5), on the right side of the column flange (cf.R1, cf.R2, cf.R4 and cf.R5), on the left side of the column flange (cf.L1, cf.L2, cf.L4 and cf.L5), on the right side beam flange (bf.t.R, bf.n.R and bf.c.R), on the left side beam flange (bf.t.L, bf.n.L and bf.c.L), on both flanges of the other edge of the beam, close to the arm where the load is applied (bf.e.R and bf.e. L), and in the middle and both sides of the column web close to the root radios (cw.C1, cw.C2, cw.R1, cw.R2, cw.L1 and cw.L2).

Also inclinometers are placed in both sides of the end plate (inc.ep.R and inc.ep.L), on the column web (inc.cw), on the beam web (inc. bw) and in the arm where the torque is applied (inc.T).

As explained above, the load is applied at the edge of an arm, which is attached to the beam edge. The load is applied until the end of the path of the hydraulic jack since the specimen is quite ductile and collapse is not reached in any of the tests. However, the beam web shows a high twist with high yielding.

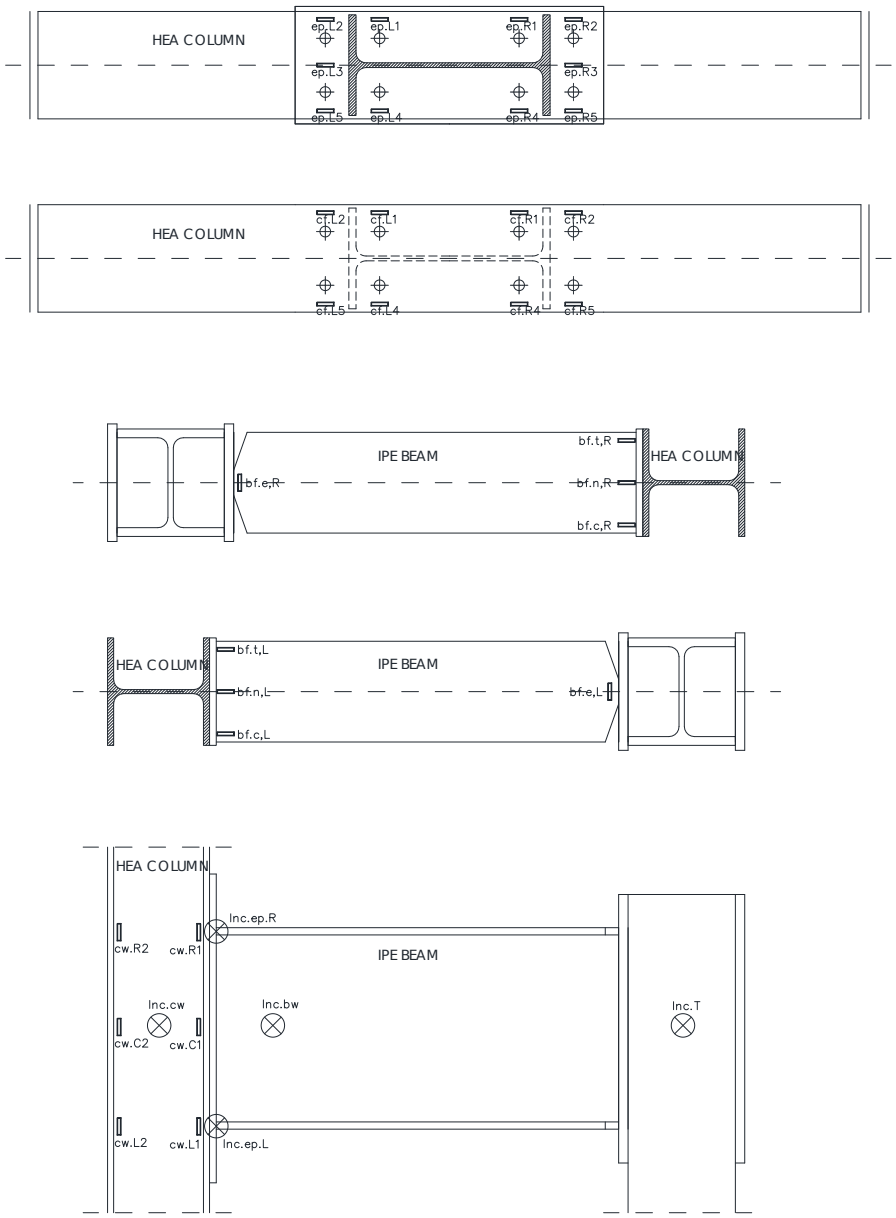

Fig. 4: Test instrumentation

2.3. Experimental results

Figs. 5 and 6 show the applied torque versus rotation curves for each specimen. Although five inclinometers were placed in each specimen, the graphs only show the more significant values. The curve for the arm where the load is applied is useful only to match the finite element curve with the experimental results. The column web curve helps to prove that the column rotation in the middle is insignificant. Also, one of the end plate curves is redundant since both sides are almost equal. This is why only the beam web rotation and one end plate

rotation are shown. However, in the case of the test TT01 the curve for the end plate is not shown since the data acquisition failed in those inclinometers.

The two specimens behave in a very similar way. None of the joints fail and both behave in a very ductile manner. A very large beam rotation is needed in order to get a small rotation in the joint. This means that the torsional stiffness of the beam is quite low when compared to the Saint-Venant torsional stiffness of the connection. This is also the reason why the beam yields before the joint in both cases.

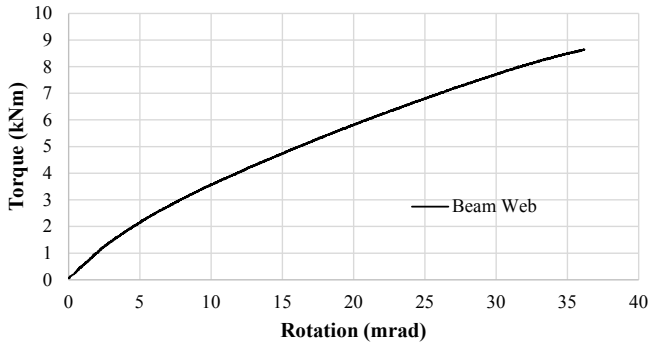

Fig. 5: Applied torque vs. rotation curve for test TT01

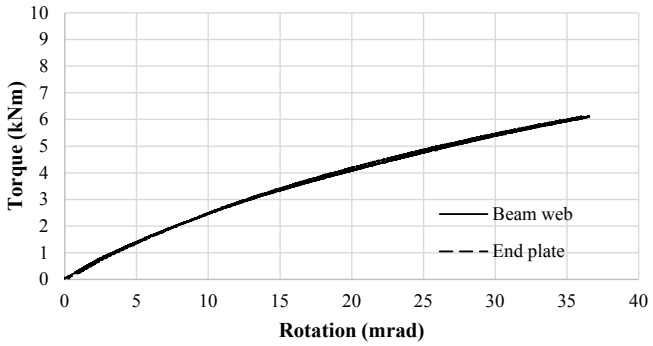

Fig. 6: Applied torque vs. rotation curve for test TT02

It may be observed in Figs. 5 and 6 that the behaviour is almost nonlinear from the outset, with a short elastic range in all the curves. As expected, the torque applied in the test TT01 is higher than the one applied in TT02 since the steel column and beam sections are larger.

Fig. 7 show the strains provided by the gauges placed in one half of the column web and column flange of the test TT01. Yielding occurs in both the column web and flange, which become the most influential of all the components. The end plate and beam flange also yield but after the yielding of the previous ones. The strain curves of the TT02 components are not shown since they are quite similar to those of the TT01 test.

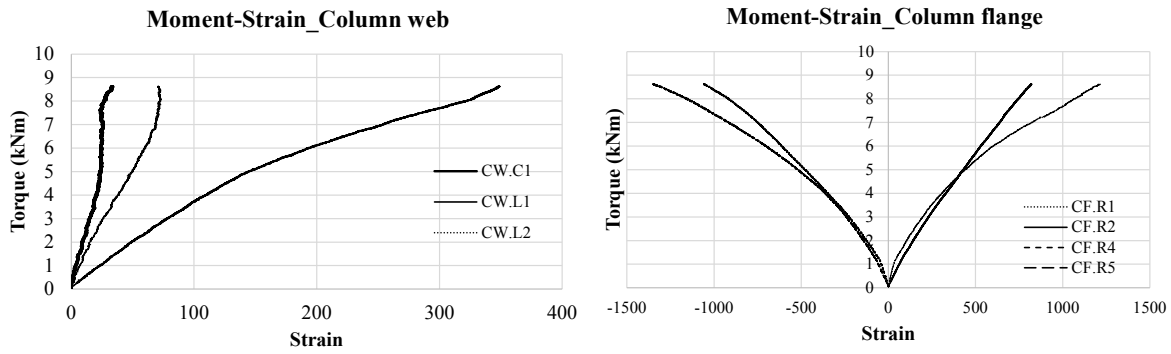

Fig. 7: Applied torque vs. strain in the column web and column flange of TT01

It is worth mentioning that the combinations of beam sections and joint properties necessary to make the connection fail instead of the beam were also studied. However, the resulting combinations were not representative of realistic joints, and therefore they were not considered as part of the study and experimental tests. In addition, since the research group has a wide experience in the calibration of FE models with experimental results, it was considered that it was not relevant to conduct more tests, which would yield redundant results.

3. Comparison with FEM Analysis

Finite element simulations are used to broaden and expand the range of cases, since a more extensive experimental program would increase the cost and human resources in a significant way. For that purpose, the finite element models have been calibrated with the experimental results before carrying out a parametric study. To this end the two specimens have been modelled by means of finite elements using the software ABAQUS [14]. The same geometry and boundary conditions of the tests have been reproduced to accurately calibrate these models with the experimental results, as described below.

3.1. Geometry, definition of the elements and boundary conditions

The three-dimensional finite element models have the same geometrical characteristics as those of the two test specimens. Beam, column, plates and bolts are modelled with the ABAQUS 8-node solid elements with reduced integration (C3D8R).

The interaction between the different parts of the joint are modelled in the following way:

- Interaction between the end plate and the column flange: surface-to-surface contact with “hard contact” in the normal direction allowing surfaces to be separated after contact.

- The nut, rod and head of the bolt were modelled as only one part in the models. The surfaces between the end plate and nut, as well as the column flange and bolt heads are tied instead of using surface-to-surface contact since they do not separate during the test and the bolts have been over dimensioned to prevent their failure in tension (Mode 3 in Eurocode 3, part 1-8 [16]) or shear. This procedure was also used by Lam and Fu [17] and Gil et al [18, 19] providing precise results and leading to a much lesser computational effort when comparing with models that include the surface contact interactions.

Regarding the boundary conditions: the column is clamped in both edges and a load is applied through an arm attached to the beam and made with a HEB profile. The purpose of this arm is to introduce a torque in the beam as done in the experimental tests.

3.2. Mesh

The mesh of the models is quite refined in all the parts, however the parts where the components yield have an even more refined mesh. The seed size is 5 mm for the column, beam and end plate. A coarser mesh (20 mm) was selected for the arm where the load is applied because its deformation is not relevant, thus an unnecessary computational effort is avoided.

As a result, the total number of elements for the model TT01 is 102922, total number of nodes is 152822 and total number of degrees of freedom is 450162. For TT02, the total number of elements is 75156, total number of nodes is 109276 and total number of degrees of freedom is 321132.

3.3. Materials

As mentioned above, the true stress-strain curves obtained from the data out of the coupon tests were introduced in the model. These values are shown in Table 2 and an example of a stress vs. strain curve is shown in Fig. 3.

3.4. Analysis

A material and geometric non-linear static analysis is carried out imposing an increasing vertical load at the end of the arm. Riks method is used as the solution control algorithm with geometric and material nonlinearities. This method allows monitoring any drops in the load-deformation curves.

3.5. Calibration of the finite element models

The experimental and finite element results are shown together in Figs. 8 and 9, respectively. The terms T_test and T_fem indicate the torque-rotation curves (obtained by test and finite elements, respectively) of the arm where the force is applied. The moment in the arm becomes the torque applied in the beam. Bw_test and Bw_fem indicate the torque-rotation curves (by test and finite elements) measured in the beam web close to the end plate. EP_test and EP_fem indicate the torque-rotation curve of the end plate. The graphs 8c, 8d, 9c and 9d show the torque vs. strain curves for the column flange (designated as CF), and end plate (designated as EP) whose locations are shown in Fig. 4.

The finite element and the experimental curves match quite well, which confirms the finite element models as a good tool to replace a wider experimental program.

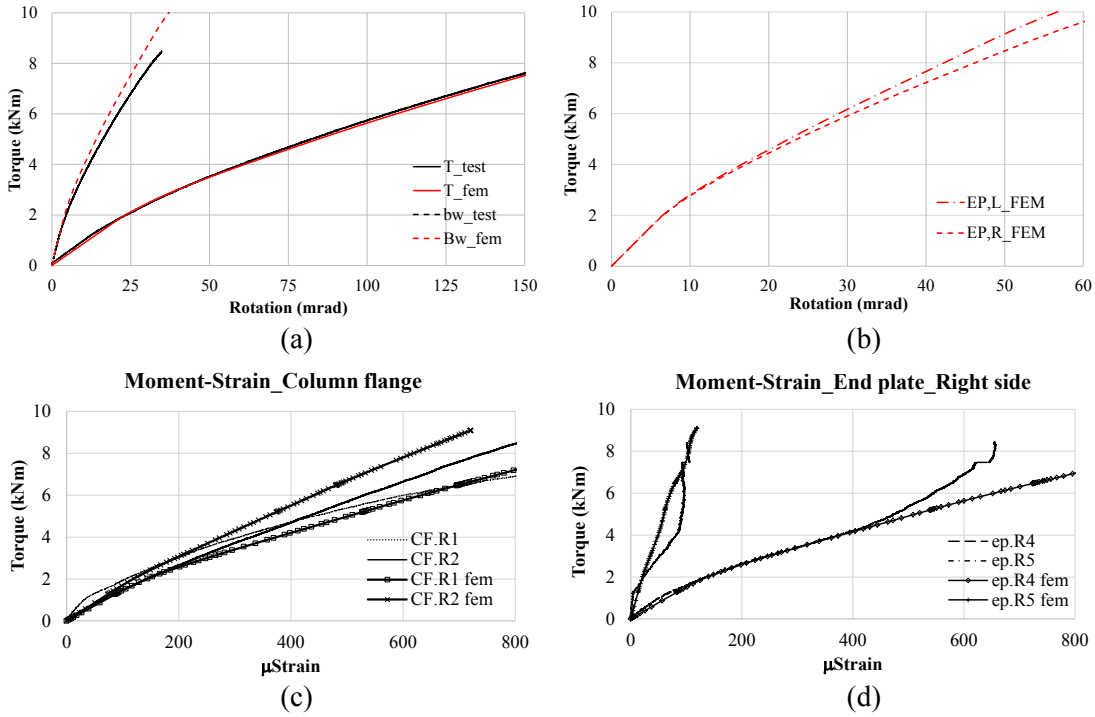

Fig. 8: Comparisons between test TT01and FEM

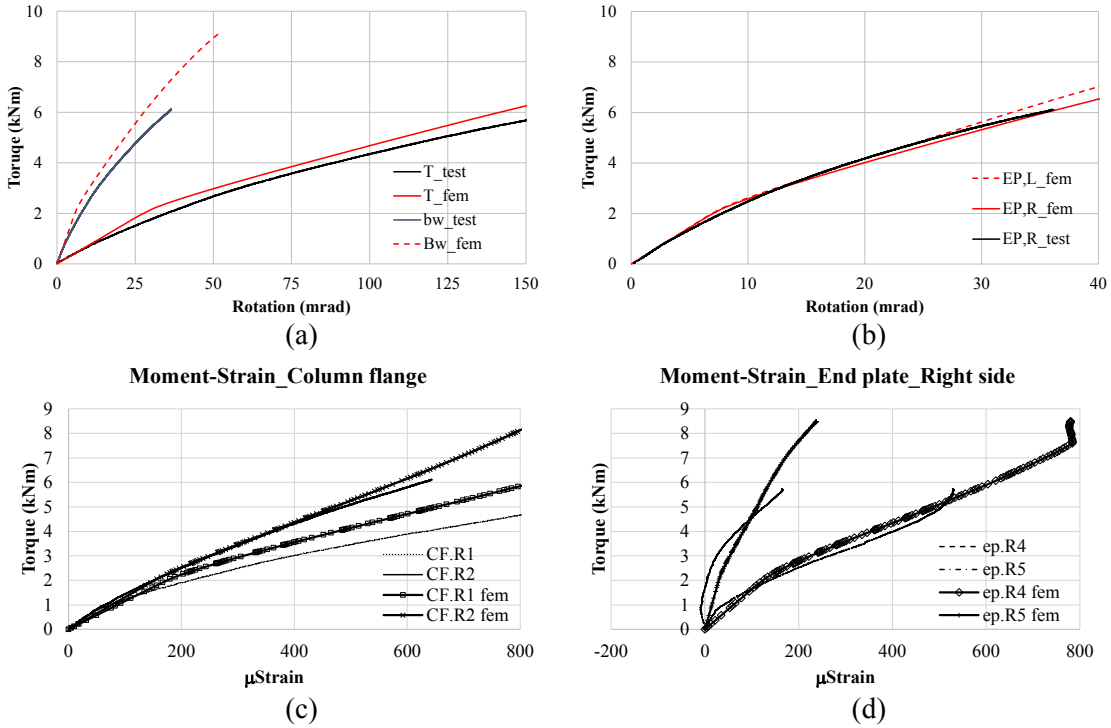

Fig. 9: Comparisons between test TT02and FEM

4. Parametric study

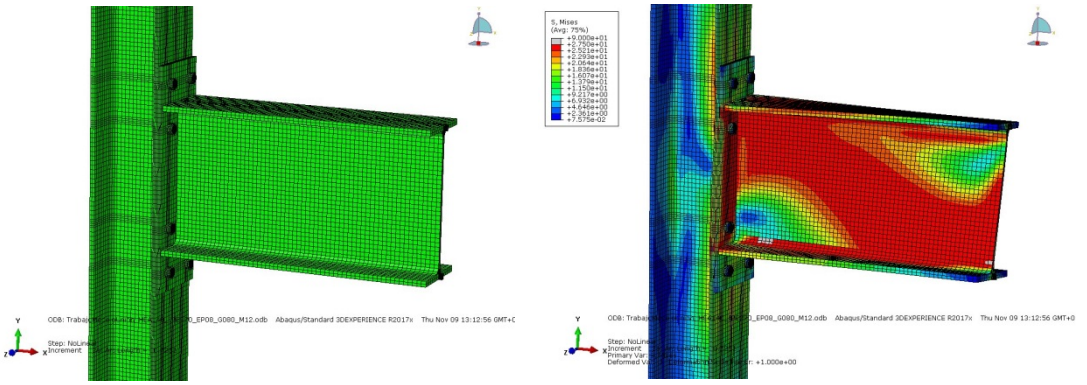

Fig. 10: Finite element model for the parametric study

A parametric study is carried out to investigate the new components involved in this kind of joint under torsion. The models have been calibrated previously against the experimental results. The study consists of thirty-two models divided in four groups of equal beam size. The models of the parametric study are slighted modified with respect to those for the calibration with the experimental results. The modification consists in excluding the loading arm, which is away from the area of interest, and to concentrate the modelling process on the behaviour of the joint, thus avoiding an unnecessary computational effort. As a consequence,

two forces are applied in both beam flanges instead of applying the torque by means of an arm (see Fig. 10). In all the cases of the parametric study, the columns are 2 m high and the beams are 0.5 m long.

Table 3 summarizes the characteristics of the 32 models. Fig. 10 shows one of the models and Fig. 11 shows the parameters that vary in the study.

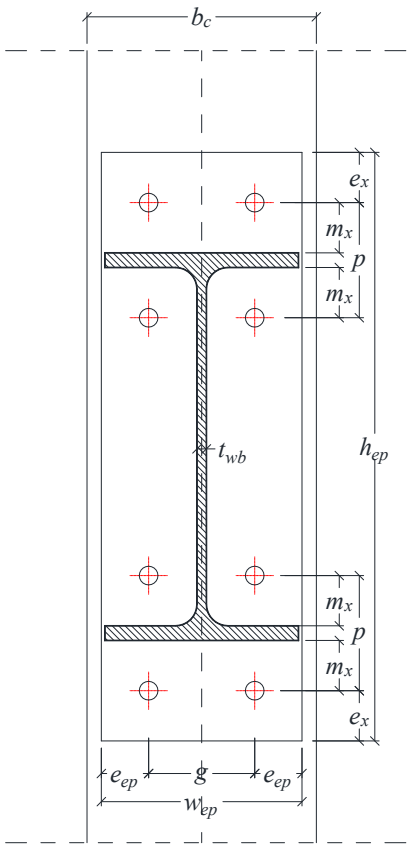

Fig. 11: Parameters of the connection subjected to torsion

The type of the elements, column boundary conditions, interactions, meshing and type of analysis are the same as in the calibrated models. However, the material behaviour is characterized by elastic-plastic bilinear curves with nominal values instead of the true stress vs. strain curves. The true stress strain curves were used to validate the finite element models. However, the aim of the parametric analysis is to predict the behavior for general cases (once the models have been validated) the parametric study is thus performed using nominal values.

Table 3: Models for the parametric study.

Model	Column	Column Length (mm)	Beam	Beam Length (mm)	End plate thickness (mm)	End plate height (mm)	End plate width (mm)	Bolts	g	eep	p	mx	ex
HEA140-IPE270-EP8-G80-M12	HEA 140	2000	IPE 270	500	8	410	140	M 12	80	30	80.2	35	35
HEA140-IPE270-EP8-G60-M12	HEA 140	2000	IPE 270	500	8	410	140	M 12	60	40	80.2	35	35
HEA140-IPE270-EP12-G80-M12	HEA 140	2000	IPE 270	500	12	410	140	M 12	80	30	80.2	35	35
HEA140-IPE270-EP12-G60-M12	HEA 140	2000	IPE 270	500	12	410	140	M 12	60	40	80.2	35	35
HEB140-IPE270-EP8-G80-M12	HEB 140	2000	IPE 270	500	8	410	140	M 12	80	30	80.2	35	35
HEB140-IPE270-EP8-G60-M12	HEB 140	2000	IPE 270	500	8	410	140	M 12	60	40	80.2	35	35
HEB140-IPE270-EP12-G80-M12	HEB 140	2000	IPE 270	500	12	410	140	M 12	80	30	80.2	35	35
HEB140-IPE270-EP12-G60-M12	HEB 140	2000	IPE 270	500	12	410	140	M 12	60	40	80.2	35	35
HEA180-IPE330-EP10-G100-M16	HEA 180	2000	IPE 330	500	10	470	180	M 16	100	40	81.5	35	35
HEA180-IPE330-EP10-G80-M16	HEA 180	2000	IPE 330	500	10	470	180	M 16	80	50	81.5	35	35
HEA180-IPE330-EP14-G100-M16	HEA 180	2000	IPE 330	500	14	470	180	M 16	100	40	81.5	35	35
HEA180-IPE330-EP14-G80-M16	HEA 180	2000	IPE 330	500	14	470	180	M 16	80	50	81.5	35	35
HEB180-IPE330-EP10-G100-M16	HEB 180	2000	IPE 330	500	10	470	180	M 16	100	40	81.5	35	35
HEB180-IPE330-EP10-G80-M16	HEB 180	2000	IPE 330	500	10	470	180	M 16	80	50	81.5	35	35
HEB180-IPE330-EP14-G100-M16	HEB 180	2000	IPE 330	500	14	470	180	M 16	100	40	81.5	35	35
HEB180-IPE330-EP14-G80-M16	HEB 180	2000	IPE 330	500	14	470	180	M 16	80	50	81.5	35	35
HEA200-IPE400-EP12-G120-M16	HEA 200	2000	IPE 400	500	12	550	200	M 16	120	40	83.5	35	40
HEA200-IPE400-EP12-G100-M16	HEA 200	2000	IPE 400	500	12	550	200	M 16	100	50	83.5	35	40
HEA200-IPE400-EP16-G120-M16	HEA 200	2000	IPE 400	500	16	550	200	M 16	120	40	83.5	35	40
HEA200-IPE400-EP16-G100-M16	HEA 200	2000	IPE 400	500	16	550	200	M 16	100	50	83.5	35	40
HEB200-IPE400-EP12-G120-M16	HEB 200	2000	IPE 400	500	12	550	200	M 16	120	40	83.5	35	40
HEB200-IPE400-EP12-G100-M16	HEB 200	2000	IPE 400	500	12	550	200	M 16	100	50	83.5	35	40
HEB200-IPE400-EP16-G120-M16	HEB 200	2000	IPE 400	500	16	550	200	M 16	120	40	83.5	35	40
HEB200-IPE400-EP16-G100-M16	HEB 200	2000	IPE 400	500	16	550	200	M 16	100	50	83.5	35	40
HEA220-IPE500-EP12-G140-M16	HEA 220	2000	IPE 500	500	12	650	220	M 16	140	40	86	35	40
HEA220-IPE500-EP12-G120-M16	HEA 220	2000	IPE 500	500	12	650	220	M 16	120	50	86	35	40
HEA220-IPE500-EP16-G140-M16	HEA 220	2000	IPE 500	500	16	650	220	M 16	140	40	86	35	40
HEA220-IPE500-EP16-G120-M16	HEA 220	2000	IPE 500	500	16	650	220	M 16	120	50	86	35	40
HEB220-IPE500-EP12-G140-M16	HEB 220	2000	IPE 500	500	12	650	220	M 16	140	40	86	35	40
HEB220-IPE500-EP12-G120-M16	HEB 220	2000	IPE 500	500	12	650	220	M 16	120	50	86	35	40
HEB220-IPE500-EP16-G140-M16	HEB 220	2000	IPE 500	500	16	650	220	M 16	140	40	86	35	40
HEB220-IPE500-EP16-G120-M16	HEB 220	2000	IPE 500	500	16	650	220	M 16	120	50	86	35	40

The addressed results are:

- Torque vs. rotation curve of the column flange at the level of both beam flanges. Both curves are equal (in absolute values) since the joint is symmetrical. Only one of them is shown.
- Torque vs. rotation curve of the end plate at the level of both beam flanges. Both curves are equal (in absolute values) since the joint is symmetrical. Only one of them is shown.
- Torque vs. rotation curve of both beam flanges, close to the end plate. Both curves are the same (in absolute values) since the joint is symmetrical, and consequently, only one of them is shown.
- Torque vs. rotation curve of the middle of the beam web close to the end plate.
- Torque vs. rotation curve of the column web in the middle of its length. This curve was obtained to verify that this rotation is null, and since it is zero is not shown in the paper.

The next section recaps the representative results of the parametric study.

4.1. Results of the parametric study

The graphs depicted in Figs. 12 to 15 show the moment-rotation curves of the 32 models, divided in the four groups of equal beam size. As expected, both the stiffness and strength of the connection are higher when it involves a HEB section than when it involves a HEA section of the same size (the HEB sections have thicker flanges and webs that the HEA sections). Also, the thicker the end plates the higher the values of stiffness and strength. Moreover and as expected, the bigger the sizes of the columns and beams the better the behaviour of the connection. The distance between bolts “g” has hardly any influence in the performance of the joint under torsion.

For all the connections, the moment rotation curves tend to be bilinear although the second branch still has a considerable slope. Also, in all of them, the beams fail before the connection, and as a consequence the curves do not show the real rotation capacity of the joint since the simulation stops at the time of the beam failure.

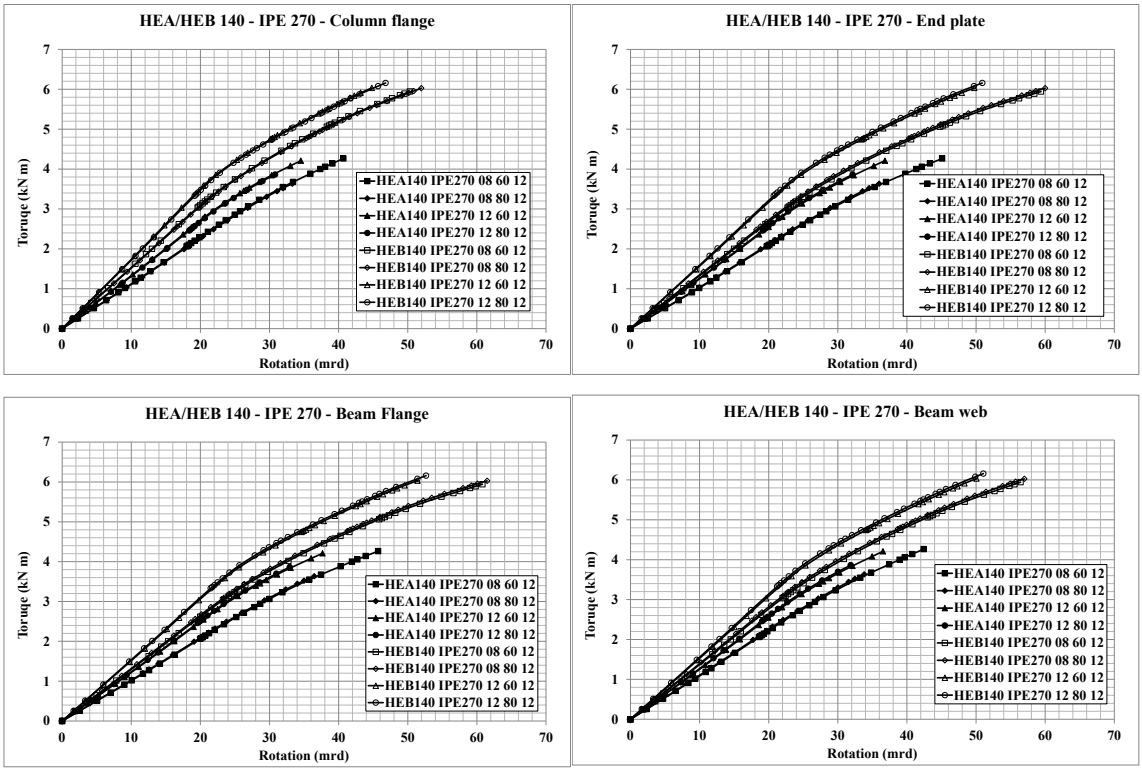

Fig.12: Moment vs. rotation curves for the first block:

HEA/HEB 140-IPE 270-EP 8/12-g60/80

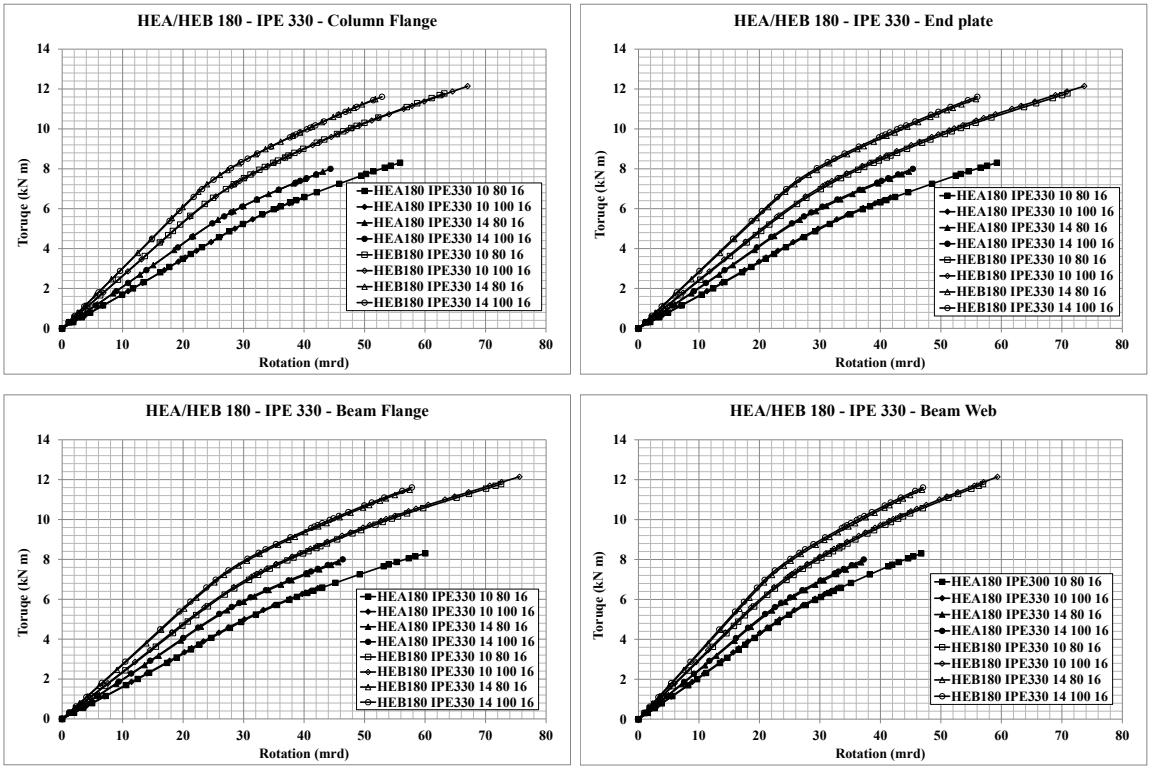

Fig.13: Moment vs. rotation curves for the second block:

HEA/HEB 180-IPE 330-EP 10/14-g80/100

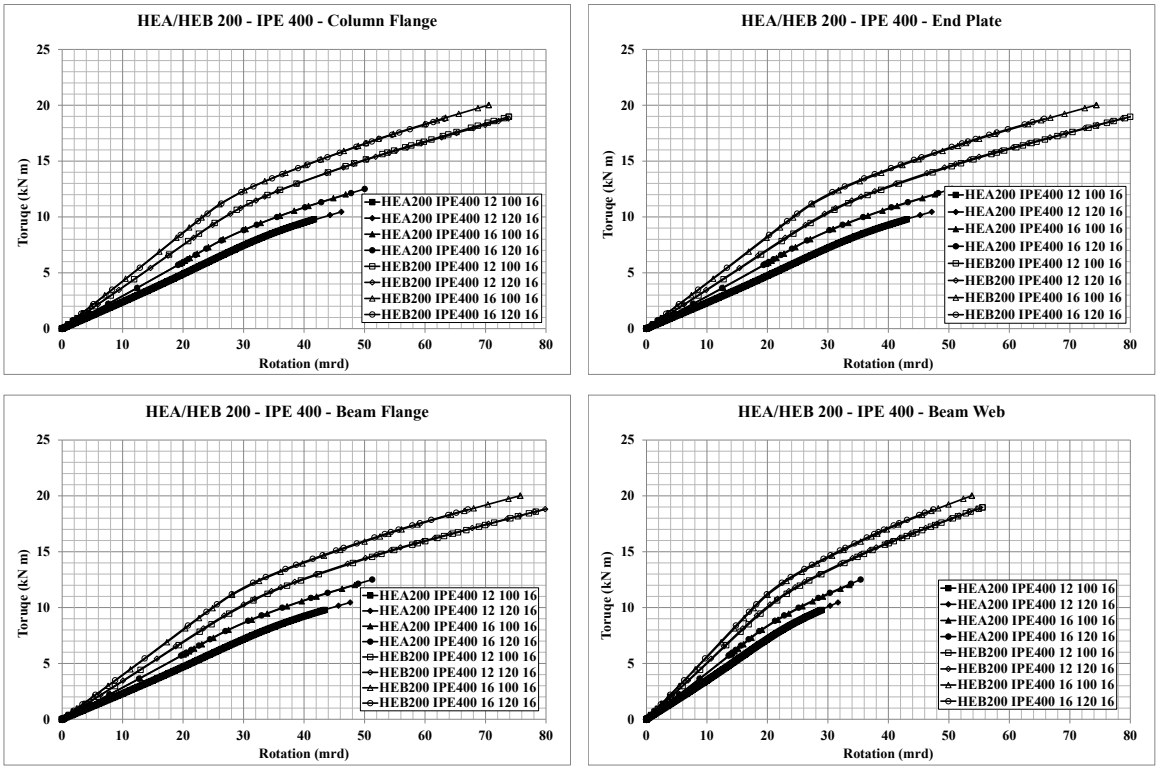

Fig.14: Moment vs. rotation curves for the third block:

HEA/HEB 200-IPE 400-EP 12/16-g120/140

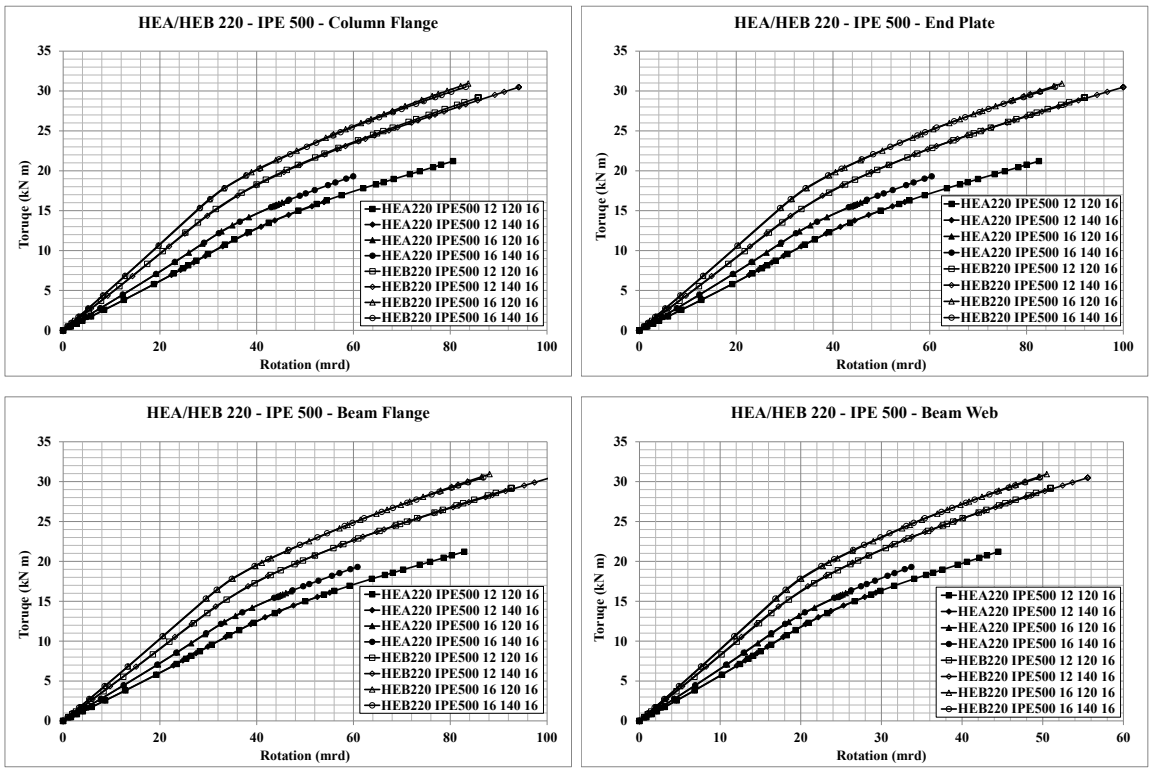

Fig.15: Moment vs. rotation curves for the fourth block:

HEA/HEB 220-IPE 500-EP 12/16-g120/140

If the joint fully prevented warping, the warping moment could be easily estimated by means of standard structural analysis procedures [20]. However, the fact that there is warping deformation in the beam flanges right at the connection, makes the joint behaviour semi-rigid and the total applied torque is composed of a uniform (Saint-Venant) part and a warping part that depends on the warping characteristics and the stiffness component shown in Fig. 16.

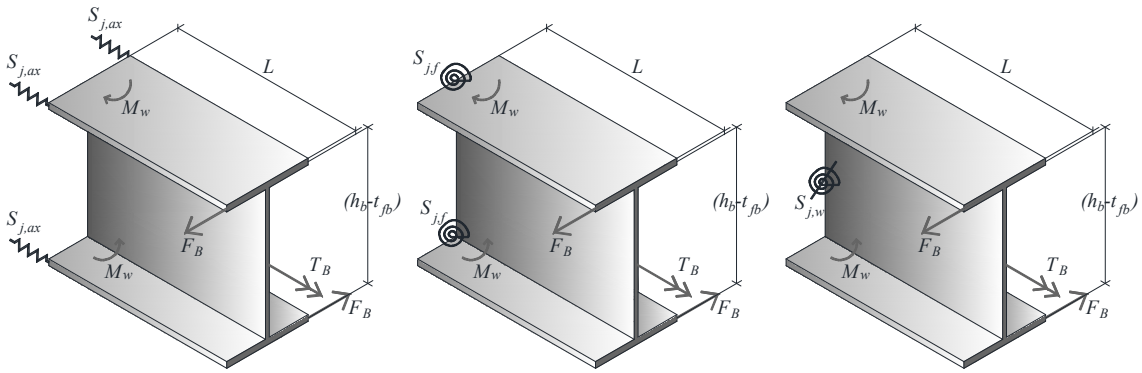

Fig. 16: Model to study the warping rotational stiffness.

To find out the warping characteristics for each model, a new finite element model is used. The model represents the beam with the same load applied in one end and translational springs in each beam flange edge as shown in Fig. 16. The springs model the stiffness of the connection concerning the warping effect. A rigid-surface constraint (available in Abaqus) is used for the beam flanges, for which the middle point of the flange becomes the control point. In this way, it is assured that the edges of the beam flanges deform as rigid surfaces, and that there are no local deformations in the nodes where the springs are attached.

The stiffness of these springs is found by iteration until the moment-rotation curve matches that of the complete model. Then, the translational stiffness $S_{j,ax}$ is transformed to a rotational spring for each beam flange or T-stub (see Fig. 16), as follows:

$$S_{j,f} = S_{j,ax}(0.5b_b)^2 \tag{1}$$

Finally, the rotational stiffness of the T-stub $S_{j,f}$ is transformed to the warping stiffness $S_{j,w}$ of the complete joint by means of the following expression:

$$S_{j,w} = S_{j,f}(h_b - t_f)^2 \tag{2}$$

Both values are shown in Table 4. If the structural analysis software allows using the first derivative of rotation as degree of freedom, which is the degree of freedom associated to the bimoment, the warping stiffness $S_{j,w}$ can be used directly. Otherwise, a mechanical model with the rotational stiffness for each T-stub under torsion $S_{j,f}$ should be used instead. As mentioned above the resistant torque under warping cannot be obtained in this study, since the beam fails under torsion before the connection in most of the cases.

Once the torsional stiffness of the connection has been obtained, it must be compared with that of the beam under torsion to assess whether the connection is semi-rigid. Analogous limits to the ones provided by the EC3 for bending must be established to classify the semi-rigid behaviour of these joints under torsion.

Table 4. Warping stiffness

FE Model	**T-Stub stiffness** $S_{j,f}$ (kNm)	**Joint Warping stiffness** $S_{j,w}$ (kNm^3)
HEA140-IPE270-EP8-G80-M12	88	5.9
HEA140-IPE270-EP8-G60-M12	85	5.7
HEA140-IPE270-EP12-G80-M12	128	8.6
HEA140-IPE270-EP12-G60-M12	124	8.4
HEB140-IPE270-EP8-G80-M12	139	9.4
HEB140-IPE270-EP8-G60-M12	136	9.2
HEB140-IPE270-EP12-G80-M12	181	12.2
HEB140-IPE270-EP12-G60-M12	177	11.9
HEA180-IPE330-EP10-G100-M16	140	14.2
HEA180-IPE330-EP10-G80-M16	137	13.9
HEA180-IPE330-EP14-G100-M16	195	19.8
HEA180-IPE330-EP14-G80-M16	191	19.4
HEB180-IPE330-EP10-G100-M16	253	25.7
HEB180-IPE330-EP10-G80-M16	247	25.1
HEB180-IPE330-EP14-G100-M16	312	31.6
HEB180-IPE330-EP14-G80-M16	306	31.0
HEA200-IPE400-EP12-G120-M16	184	27.5
HEA200-IPE400-EP12-G100-M16	184	27.5
HEA200-IPE400-EP16-G120-M16	249	37.2
HEA200-IPE400-EP16-G100-M16	247	36.9
HEB200-IPE400-EP12-G120-M16	328	49.0
HEB200-IPE400-EP12-G100-M16	314	46.9
HEB200-IPE400-EP16-G120-M16	396	59.2
HEB200-IPE400-EP16-G100-M16	385	57.5
HEA220-IPE500-EP12-G140-M16	183	42.9
HEA220-IPE500-EP12-G120-M16	177	41.5
HEA220-IPE500-EP16-G140-M16	241	56.5
HEA220-IPE500-EP16-G120-M16	240	56.2
HEB220-IPE500-EP12-G140-M16	335	78.5
HEB220-IPE500-EP12-G120-M16	332	77.8
HEB220-IPE500-EP16-G140-M16	398	93.2
HEB220-IPE500-EP16-G120-M16	395	92.5

5. Classification of the joints under torsion.

In general terms, the torsional deformation is due to the two components of the torsion: uniform or St Venant torsion (which translates into a rotation of the section) and non-uniform torsion or warping (which produces rotations in the flanges). Beams subjected to uniform torsion are primarily analysed and designed as clamped assuming that the joints are rigid under uniform torsion. However, when warping is present the warping moments induce a rotation on the beam flanges that is also translated to the column flanges. In this last scenario, the connection becomes semi-rigid.

In order to classify the joint as rigid or semi-rigid, the torsional characteristics of the joint should be compared with the beam torsional and warping stiffness. In the case of the type of connection under study, its uniform torsional rotation can be considered negligible (except for a possible slip of the bolts in the bolt-holes that is considered irrelevant for the purpose of this study). Therefore, these connections can be considered as rigid (and even full strength) regarding uniform torsion.

Therefore, the classification and possible semi-rigid behaviour will be evaluated taking into consideration the warping characteristics of both the beam and connection. The comparison will be established from the cases dealt with in the parametric study described in Section 4. With the aim of establishing a classification similar to the one of the EC3-part 1.8 (clauses 5.2.2 and 5.2.3) for joints under bending, two criteria could be considered:

1. Comparing the stiffness $S_{j,f}$ of one flange or T-stub of the joint in its minor axis with the rotational stiffness of the beam flange (or half beam) in its minor axis $S_{b,f} = \frac{EI_z}{2L}$. In this case, the limits would be the same as in EC3. Thus, if $S_{j,f} > 0.5S_{b,f}$, then the joint becomes semi-rigid in regard to warping.
2. Comparing the warping stiffness $S_{j,w}$ of the joint with the warping stiffness of the beam $S_{b,w} = \frac{\mathrm{E}I_w}{L}$, where I_w is the warping constant for a symmetrical I section and it is approximately $I_w \sim I_z(h - t_f)^2/4$. In this case, due to the relation between $S_{b,f}$ and $S_{b,w}$, the limit should be twice the limit for the previous case. Thus, if $S_{j,w} > S_{b,w}$ the joint becomes semi-rigid to warping.

Both criteria lead to the same classification. Table 4 shows the results using the second criteria, which resulted in a classification of semi-rigid for all the cases contemplated in the parametric study. In regard to strength and as mentioned above, the beam fails before the joint in all cases, and therefore, this connection can be classified as full-strength.

Table 4. Classification of the joints by warping stiffness.

Model **Without additional plates**	**Joint warping stiffness** $S_{j,w}$ kNm³	**Beam warping stiffness** $S_{b,w}$ kNm³	**Ratio** $S_{j,w}/S_{b,w}$	**Classification by stiffness**
HEA140-IPE270-EP8-G80-M12	5.9	3.3	1.8	>1. Semi-rigid
HEA140-IPE270-EP8-G60-M12	5.7	3.3	1.7	>1. Semi-rigid
HEA140-IPE270-EP12-G80-M12	8.6	3.3	2.6	>1. Semi-rigid
HEA140-IPE270-EP12-G60-M12	8.4	3.3	2.5	>1. Semi-rigid
HEB140-IPE270-EP8-G80-M12	9.4	3.3	2.8	>1. Semi-rigid
HEB140-IPE270-EP8-G60-M12	9.2	3.3	2.8	>1. Semi-rigid
HEB140-IPE270-EP12-G80-M12	12.2	3.3	3.7	>1. Semi-rigid
HEB140-IPE270-EP12-G60-M12	11.9	3.3	3.6	>1. Semi-rigid
HEA180-IPE330-EP10-G100-M16	14.2	7.0	2.0	>1. Semi-rigid
HEA180-IPE330-EP10-G80-M16	13.9	7.0	2.0	>1. Semi-rigid
HEA180-IPE330-EP14-G100-M16	19.8	7.0	2.8	>1. Semi-rigid
HEA180-IPE330-EP14-G80-M16	19.4	7.0	2.8	>1. Semi-rigid
HEB180-IPE330-EP10-G100-M16	25.7	7.0	3.7	>1. Semi-rigid
HEB180-IPE330-EP10-G80-M16	25.1	7.0	3.6	>1. Semi-rigid
HEB180-IPE330-EP14-G100-M16	31.6	7.0	4.5	>1. Semi-rigid
HEB180-IPE330-EP14-G80-M16	31.0	7.0	4.5	>1. Semi-rigid
HEA200-IPE400-EP12-G120-M16	27.5	14.7	1.9	>1. Semi-rigid
HEA200-IPE400-EP12-G100-M16	27.5	14.7	1.9	>1. Semi-rigid
HEA200-IPE400-EP16-G120-M16	37.2	14.7	2.5	>1. Semi-rigid
HEA200-IPE400-EP16-G100-M16	36.9	14.7	2.5	>1. Semi-rigid
HEB200-IPE400-EP12-G120-M16	49.0	14.7	3.3	>1. Semi-rigid
HEB200-IPE400-EP12-G100-M16	46.9	14.7	3.2	>1. Semi-rigid
HEB200-IPE400-EP16-G120-M16	59.2	14.7	4.0	>1. Semi-rigid
HEB200-IPE400-EP16-G100-M16	57.5	14.7	3.9	>1. Semi-rigid
HEA220-IPE500-EP12-G140-M16	42.9	32.8	1.3	>1. Semi-rigid
HEA220-IPE500-EP12-G120-M16	41.5	32.8	1.3	>1. Semi-rigid
HEA220-IPE500-EP16-G140-M16	56.5	32.8	1.7	>1. Semi-rigid
HEA220-IPE500-EP16-G120-M16	56.2	32.8	1.7	>1. Semi-rigid
HEB220-IPE500-EP12-G140-M16	78.5	32.8	2.4	>1. Semi-rigid
HEB220-IPE500-EP12-G120-M16	77.8	32.8	2.4	>1. Semi-rigid
HEB220-IPE500-EP16-G140-M16	93.2	32.8	2.8	>1. Semi-rigid
HEB220-IPE500-EP16-G120-M16	92.5	32.8	2.8	>1. Semi-rigid

As shown in Table 4, and as expected, the stiffness ratio between the joint and the beam stiffness is higher for the HEB columns than for the HEA. Also, the thicker the end plate is,

the higher the ratio. However, the distances between the bolts, and between bolts and edges hardly have any influence in the stiffness ratio.
Once the semi-rigid behaviour is confirmed, the components that are involved in these joints have to be characterized to predict an accurate behaviour in the structural analyses, and allow the use of advanced calculations.

6. Component modelling for stiffness and strength

The connection can be subdivided in two anti-symmetric T-stubs bending in opposite directions. Besides, due to that bending, each T-stub has a pulling and a pushing side. Accordingly, the components that are involved in the joint are:

a) End plate in bending (pull side)
b) Column flange in bending (pull side)
c) Beam flange in tension
d) Bolts: in tension, in shear and in bearing
e) End plate in bending (push side)
f) Column flange in bending (push side)
g) Beam flange in compression/buckling
h) Column flange and end plate in torsion
i) Column web in bending

Components a) to g) are already defined in the Eurocode 3 [13] and updated in reference [10]. The column flange in torsion and column web in bending are also characterized in reference [10] for the case of a single T-Stub. However, due to the presence of two anti-symmetric T-Stubs instead of an isolated T-Stub, these components need some modifications that are dealt with below.

a. Column flange and end plate in torsion

The out of plane bending of an isolated T-stub causes torsional moments in the column flange, whose distribution is shown in Fig. 17.

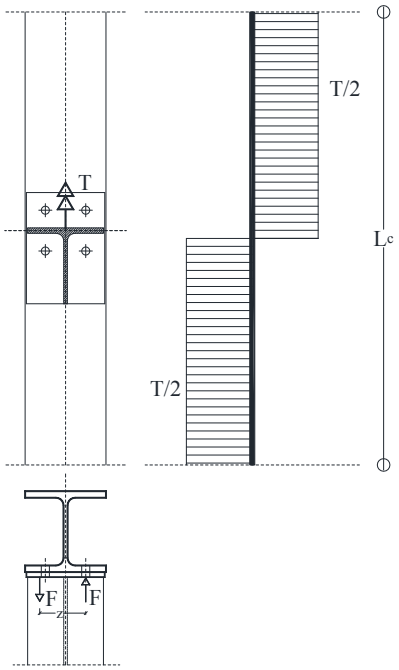

Fig. 17: Torsional moment distribution for an isolated T-Stub under out of plane bending

When there are two anti-symmetric T-stubs, the torsional moment distribution in the column flange changes, as shown in Fig. 18. The first distribution corresponds to a column with edges where the rotation is not prevented. The second distribution corresponds to a column with edges whose rotation is prevented. The latter is the normal situation and the torsional moment in the zone of the joint is:

$$T_c = M_w(L_c - h_b)/L_c \tag{3}$$

where, M_w is the minor axis moment applied in each T-Stub, that is, the warping moment; L_c is the length of the column and h_b is the height of the beam.

Since the ratio between the height of the beam (h_b) and the total height of the column (L_c) in real frames is very low, the torsional moment in the column flange, in the area of the joint, tends to be equal to the applied moment M_w in each T-Stub. For real frames, the most conservative case could be considered, where T_c is equal to M_w. However the accurate distribution should be considered for the parametric study and the analytical characterization.

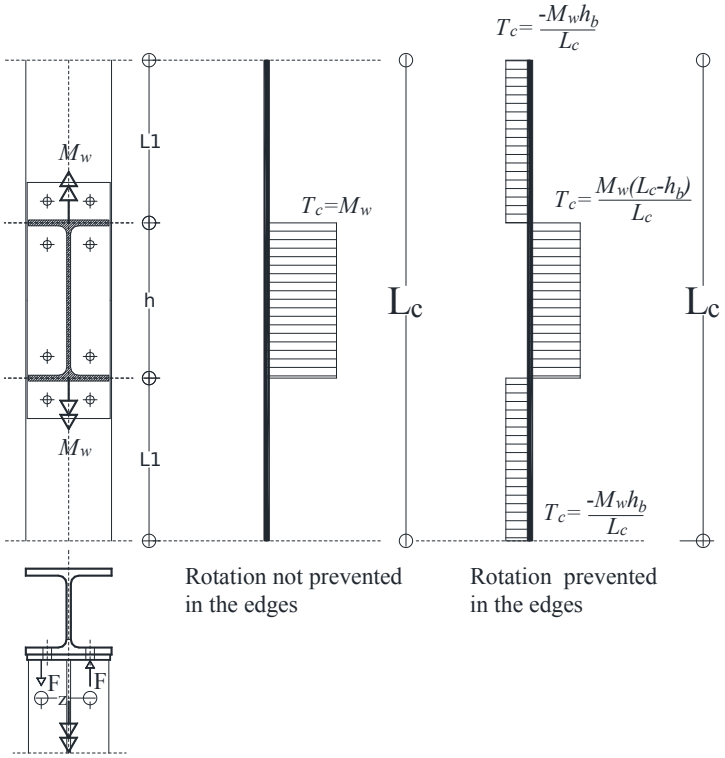

Fig. 18: Torsional moment distribution for a mayor axis connection under torsion.

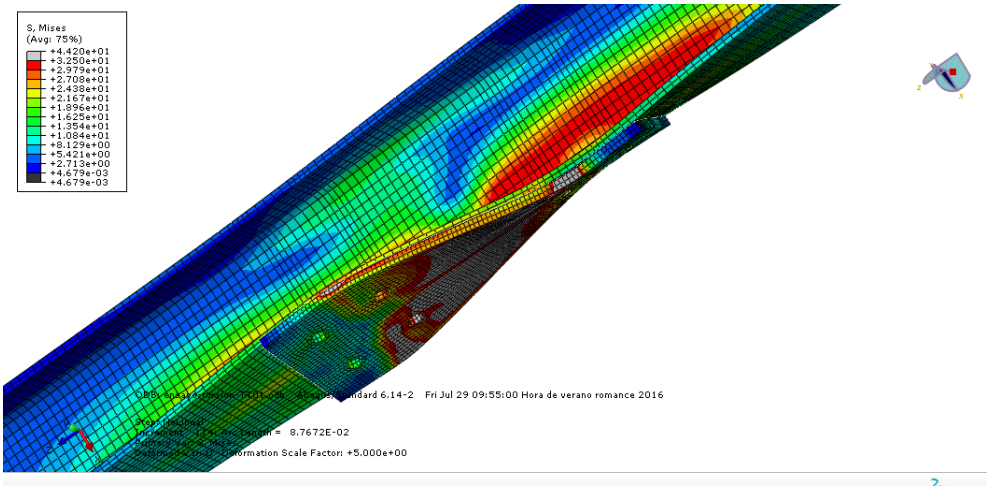

Fig. 19: Finite element model: Deformation of the column

This torsional moment T_c should not be confused with the torque applied to the beam T_B. The latter decomposes into a couple of forces F_B applied in the beam flanges which in turn cause an out-of-plane bending in each T-stub (M_w), and also induces a uniform torsional moment T_c in the column flange. The strength and stiffness of this component are developed below in an analogous way as that described in [10].

The plastic resistance of a rectangular section in torsion is $T_{pl,Rd} = W_{T,pl}\tau_y$

Where the plastic torsional modulus is $W_{T,pl} = \frac{t^2(3b_c - t)}{6}$, the maximum tangential stress is $\tau y = \frac{f_{yd}}{\sqrt{3}}$, and b_c and t are the breath and the thickness of the considered section, respectively.

The moment M_w in the T-Stub can be treated as a couple of forces F acting at a distance z, $M_w=Fz$, then $T_c = Fz(L_c - h_b)/L_c$, where z is the distance between the bolts in tension and the resultant of compression for each T-Stub (see Fig. 18**).**

And $T_{pl,Rd} = W_{pl}\tau_y = Fz(L_c - h_b)/L_c$

Consequently, the maximum force that can be applied in each side of the beam flange is:

$$F_{cf,t,Rd} = \frac{W_{T,pl}\tau_y}{z}\left(\frac{L_c}{L_c - h_b}\right) = \frac{t^2(3b_c - t)f_{yd}}{z\,6\sqrt{3}}\left(\frac{L_c}{L_c - h_b}\right) \quad (4)$$

Taking into account that the end plate and the column flange twist together (see Fig. 19), and that there is barely a slip between them because the bolts prevent it, the thickness t for the calculation of the plastic torsional modulus will be the sum of that of the column flange and the end plate, affected by a coefficient that is taken equal to 0.83 obtained by regression analysis, that is t=0.83$(t_{fc}+t_{ep})$.

Regarding the initial stiffness, the torsional rotation in the zone of the joint is $\theta = \frac{T_c h_b}{GJ}$, that is $\theta = \frac{M_w\left(L_c/L_c - h_b\right)h_b}{GJ}$; then, the rotational stiffness is $S_{rot} = \frac{GJ}{h_b}\left(\frac{L_c}{L_c - h_b}\right)$ and the axial stiffnes is

$$S_{ax} = \frac{GJ}{h_b z^2}\left(\frac{L_c}{L_c - h_b}\right) = \frac{0.38EJ}{h_b z^2}\left(\frac{L_c}{L_c - h_b}\right) \quad (5)$$

Therefore, the component stiffness coefficient is:

$$k_{cf,T} = \frac{0.38J}{h_b z^2}\left(\frac{L_c}{L_c - h_b}\right) \quad (6)$$

where, h_b is the length of the column where the torsional moment T_c acts. In this case is equal to the height of the beam, z is the lever arm (distance between the bolts in tension and the centre of compression) and J is the torsional modulus of the considered section: $J = \frac{1}{3}b_c t^3$, where the thickness t will be the same as for the strength, that is t=0.83$(t_{fc}+t_{ep})$.

b. Column web in bending

The column web also undergoes anti-symmetric bending in the transversal direction, as it is shown in Fig. 20. (The scale is augmented in order to observe the bending).

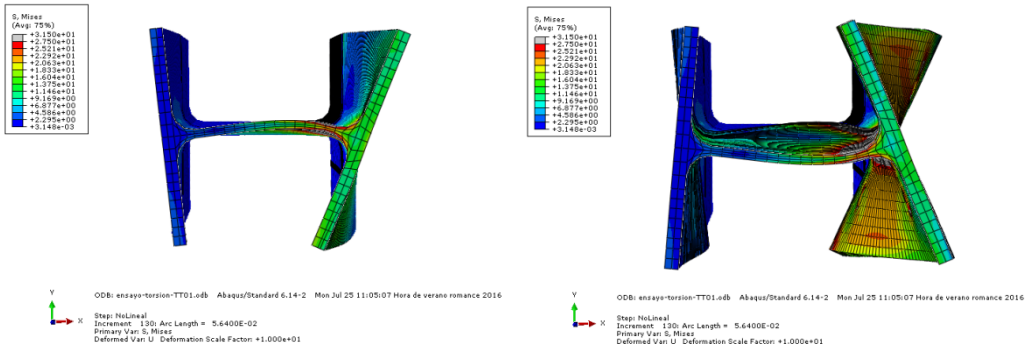

Fig.20: Bending in the column web

The bending in the transversal direction can be characterized as in [10] but the effective length has to be modified for the upper half beam and the lower one. Consequently, the effective length $l_{eff,cw,b}$ for each anti-symmetric T-Stub will be half the length of the isolated T-Stub plus half the height of the beam.

For the sake of completeness the formula for the strength of the column web in bending that appears in reference [10] is also included here as follows:

$$F_{cw,b,Rd} = \frac{M_{pl,cw,Rd}}{z} = \frac{l_{eff,cw,b} t_{wc}^{\ 2} f_{yd}}{4z} \qquad (7)$$

where:

$M_{pl,cw,Rd}$ is the plastic resistant moment of the effective section of the column web

z is the lever arm

g is the distance between bolts, measured horizontally

$l_{eff,cw,b}$ is the effective length for the column web in bending, $l_{eff,cw,b} = 0.5 l_{eff,cw,Tstub,b} + 0.5 h_b$ as explained above, where the rest of the parameters are defined in reference [10] with the following equations: $l_{eff,cw,Tstub,b} = 2 l_{eff,cf,b}$; $l_{eff,cf,b} = (5{,}5 m_l + 4 e_l + p_l)$; $m_l = (0{,}5 b_{ep} - 0{,}5 t_{wc} - 0{,}8 r_c)/2$; $e_l = 0{,}5 b_c - m_l - (0{,}5 t_{wc} + 0{,}8 r_c)$; $p_l = t_{fb} + 2 a_w \sqrt{2} + 2 t_{ep}$.

Concerning the stiffness, unlike what happened in the isolated T-Stub [10], the rotational spring in one column flange is different to the opposite one since one of them corresponds to the column flange in torsion alone and the other one corresponds to the column flange bending together with the end plate ($k_{1cf,t}$ and $k_{2cf,t}$ respectively in Fig. 21).

Then, the stiffness coefficient for the column web in bending can be calculated by means of standard structural analysis as:

$$k_{cw,b} = \frac{1}{z^2}\left(\frac{-4I_{cw}{}^2}{d_c\left(4I_{cw} + k_{1cf,t}d_c z^2\right)} + \frac{\left(4I_{cw} + k_{2cf,t}d_c z^2\right)}{d_c}\right) \tag{8}$$

where, I_{cw} is the inertia of the effective section of the column web $I_{cw} = \frac{l_{eff,cw,b}t_{wc}{}^3}{12}$

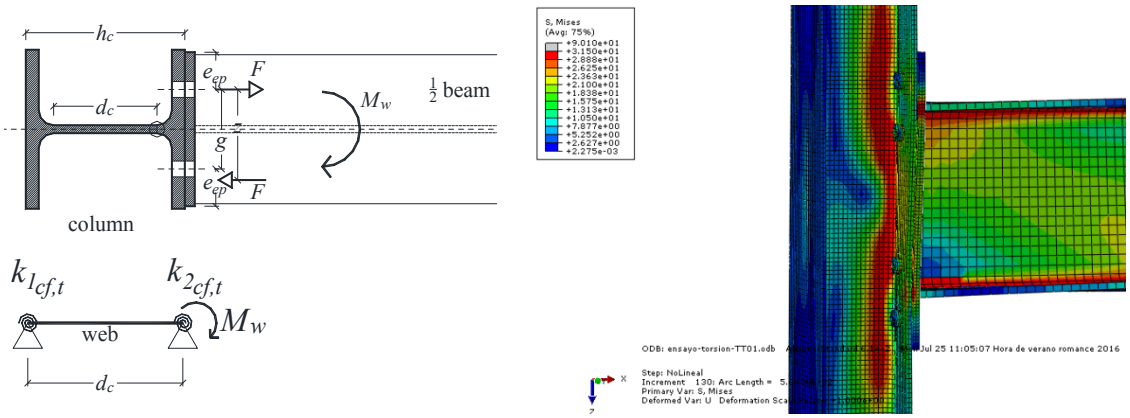

Fig.21: Analytical model for the column web in bending

7. Mechanical model

After the modification of the components, Fig. 22 shows the proposed mechanical model. The components in the pull side (column flange in bending (cf,b,t) end plate in bending (ep,b,t) and bolts in tension (b,t)) are assembled in series, meanwhile for the push side the component end plate in bending (ep,b,c) is assembled with the column flange in bending (cf,b,c) in parallel, and later assembled in series with the beam flange in compression (bf,c) or buckling; according to what is specified in EC3, part 1-8 [16]. They all are assembled with the column web in bending, which also includes the column flange plus end plate in torsion.

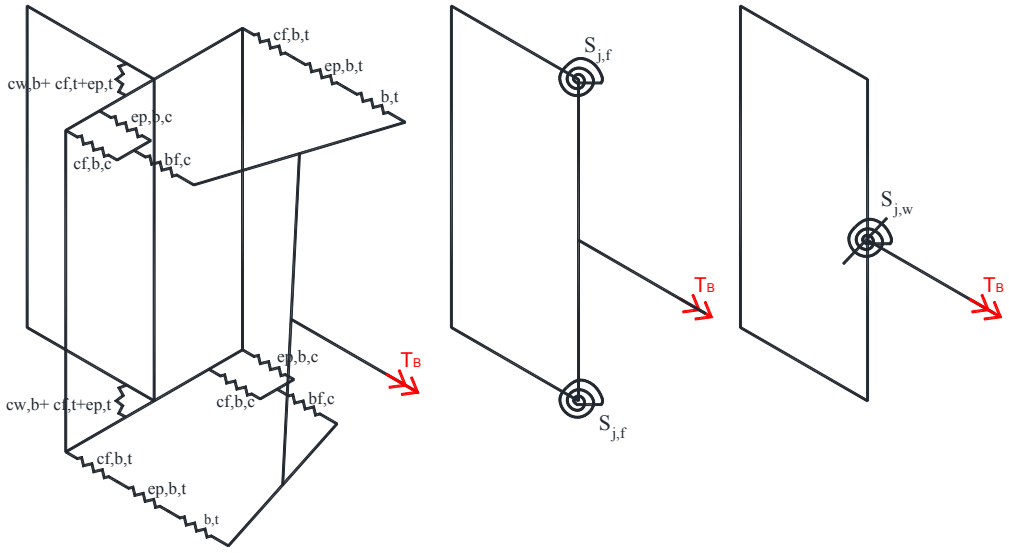

Fig.22: Mechanical model for the two anti-symmetric T-Stubs

Finally, the rotational stiffness and strength are found for each anti-symmetric T-stub.

To transform this stiffness to the one corresponding to the bimoment associated to the first derivative of the section rotation, the following expression can be used $S_{j,w} = S_{j,f}(h - t_f)^2$

And to transform the warping moment in the flange M_w to the bimoment B associated to the first derivative of rotation, the following formula applies: $B = M_w(h - t_f)$.

Table 5: Warping stiffness and comparison with the analytical results and warping moment.

	Intial Warping Stiffness $S_{i,w}$ (kNm)			**Resistance M_w (kNm)**
Model	**FEM**	**Analytical**	**Error %**	**Analytical**
HEA140-IPE270-EP8-G80-M12	5.9	5.1	14.5%	4.3
HEA140-IPE270-EP8-G60-M12	5.7	5.1	10.1%	4.3
HEA140-IPE270-EP12-G80-M12	8.6	7.5	13.4%	6.1
HEA140-IPE270-EP12-G60-M12	8.4	7.5	10.8%	6.1
HEB140-IPE270-EP8-G80-M12	9.4	9.4	0.0%	6.3
HEB140-IPE270-EP8-G60-M12	9.2	9.6	4.5%	6.3
HEB140-IPE270-EP12-G80-M12	12.2	12.8	4.9%	8.5
HEB140-IPE270-EP12-G60-M12	11.9	12.7	6.3%	8.5
HEA180-IPE330-EP10-G100-M16	14.2	11.7	18.0%	7.5
HEA180-IPE330-EP10-G80-M16	13.9	11.8	15.5%	7.5
HEA180-IPE330-EP14-G100-M16	19.8	16.9	14.5%	10.3
HEA180-IPE330-EP14-G80-M16	19.4	17.0	12.0%	10.3
HEB180-IPE330-EP10-G100-M16	25.7	25.1	2.2%	11.3
HEB180-IPE330-EP10-G80-M16	25.1	25.6	2.1%	11.3
HEB180-IPE330-EP14-G100-M16	31.6	33.0	4.4%	15.3
HEB180-IPE330-EP14-G80-M16	31.0	33.1	6.5%	15.3

HEA200-IPE400-EP12-G120-M16	27.5	23.2	15.6%	11.2
HEA200-IPE400-EP12-G100-M16	27.5	23.5	14.7%	11.2
HEA200-IPE400-EP16-G120-M16	37.2	32.4	13.0%	14.8
HEA200-IPE400-EP16-G100-M16	36.9	32.7	11.3%	14.8
HEB200-IPE400-EP12-G120-M16	49.0	48.3	1.4%	15.9
HEB200-IPE400-EP12-G100-M16	46.9	49.1	4.7%	15.9
HEB200-IPE400-EP16-G120-M16	59.2	62.1	5.0%	20.0
HEB200-IPE400-EP16-G100-M16	57.5	62.4	8.5%	21.7
HEA220-IPE500-EP12-G140-M16	42.9	41.9	2.4%	13.4
HEA220-IPE500-EP12-G120-M16	41.5	42.4	2.4%	14.4
HEA220-IPE500-EP16-G140-M16	56.5	56.8	0.7%	18.9
HEA220-IPE500-EP16-G120-M16	56.2	57.3	2.1%	18.9
HEB220-IPE500-EP12-G140-M16	78.5	84.1	7.1%	13.5
HEB220-IPE500-EP12-G120-M16	77.8	86.1	10.7%	15.7
HEB220-IPE500-EP16-G140-M16	93.2	107.1	14.7%	21.0
HEB220-IPE500-EP16-G120-M16	92.5	108.1	16.7%	23.1
AVERAGE ERROR			8.5%	
STANDARD DEVIATION			0.054	

8. Comparison between components based stiffness and strength with FEM.

Table 5 shows the warping stiffness calculated by means of the finite element method and by means of the proposed analytical method. Both values are quite close in most of the cases, which validates the proposed analytical method as sufficiently accurate to predict the warping initial stiffness. The average error is 8.5%, which is quite acceptable.

An assessment of the warping moment resistance in the T-Stub M_w calculated by means of the proposed method and assembled in series or in parallel according to what is specified in EC3, part 1-8 [16] is also presented in Table 5. However, it is not compared with the FEM, since the value could not be obtained due to the fact that the beam fails before the joint in most cases.

9. Conclusions.

In this research the behaviour of bolted major axis steel joints with doubled extended end plate subjected to torsion have been studied. These joints lack stiffeners or additional plates welded to the column flange, and therefore they are assumed to behave as semi-rigid.

Torsional effects are to be considered in 3D structures, in fire analysis of 2D structures, in beams bearing floors with eccentric loads, etc. Also, the stability checks according to the current codes allow the simplification of considering the joints as pinned or rigid. However, the consideration of the real boundary conditions can lead to more accurate results at the time of performing global analyses and stability checks. Furthermore, to completely define the performance of 3D joints, the joint behaviour under independent loading conditions should be known.

For the study and characterization of the joints, firstly an experimental program composed of two tests has been performed. Later, a parametric study by means of finite element models, validated with the experimental results, was carried out. In this study the beam size, column size, column type, end plate thickness, bolts diameter, and distances between bolts and plate edges have been varied.

The parametric study performed and presented in this paper verifies that these joints behave in a semi-rigid way when compared with the torsional characteristics of the attached beam. The fact that the beams fail prior to the connections in most cases prevented an evaluation of the resistance of the connection. On the other hand, this fact also demonstrates that the joints can be assumed to behave as full-strength.

These facts strengthen the importance of considering the actual characteristics of these joints. An analytical formulation for the stiffness is proposed based on both the component method and the results of reference [10] for the isolated T-stub under out of plane bending. Applying the necessary modifications for the torsional conditions and assembling the components according to a mechanical model, verification is made that the proposed formulation predicts the warping stiffness with sufficient accuracy, and with an average error of 8.5%.

In regard to the connection resistance, finite element simulations could not provide any results since the beams failed before the connection in practically all cases, thus corroborating that the joint can be classified as full-strength. Nevertheless, an analytical assessment of the resistance has been made by means of the proposed method and assembled in series or in parallel according to what is specified in EC3, part 1-8 [16].

Finally, both uniform and non-uniform torsion are conditions that are not going to happen in an isolated way very often. The most common cases will involve complex couplings and interactions with other connection forces such as axial and shear, and bending moments that can occur simultaneously in 3D joints or in 2D joints subjected to out of plane loads. These

interactions are exceedingly complicated and will require complex 3D mechanical models capable of modelling them accurately.

10. Acknowledgements.

The financial support provided by the Spanish Ministerio de Economía y Competitividad under contracts BIA2013-48069-C2-1-P and BIA2016-80358-C2-1-P is gratefully acknowledged.

11. References.

[1] Bayo E, Loureiro A, Lopez M, Simoes da Silva L. General component based cruciform finite elements to model 2D steel joints with beams of equal and different depths. Engineering Structures. 2017;152:698-708.
[2] Francavilla AB, Latour M, Piluso V, Rizzano G. Simplified finite element analysis of bolted T-stub connection components. Engineering Structures. 2015;100:656-64.
[3] Augusto H, Simoes da Silva L, Rebelo C, Castro JM. Characterization of web panel components in double-extended bolted end-plate steel joints. Journal of Constructional Steel Research. 2016;116:271-93.
[4] Gil B, Goñi R, Bayo E. Experimental and numerical validation of a new design for three-dimensional semi-rigid composite joints. Engineering Structures. 2013;48:55-69.
[5] Cabrero JM, Bayo E. The semi-rigid behaviour of three-dimensional steel beam-to-column joints subjected to proportional loading. Part I. Experimental evaluation. Journal of Constructional Steel Research. 2007;63:1241-53.
[6] Cabrero JM, Bayo E. The semi-rigid behaviour of three-dimensional steel beam-to-column joints subjected to proportional loading. Part II: Theoretical model and validation. Journal of Constructional Steel Research. 2007;63:1254-67.
[7] Loureiro A, Lopez M, Gutiérrez R, Reinosa JM. Experimental and numerical analysis of E-stubs in three dimensional joints: A new analytical formulation for the stiffness calculation. Engineering Structures. 2013;53:1-9.
[8] Loureiro A, Lopez M, Gutiérrez R, Reinosa JM. A new analytical formulation for the E-stub strength calculation in three dimensional steel joints with additional plates welded to the weak axis. Engineering Structures. 2013;56:2263-72.
[9] Gil B, Goñi R. T-stub behaviour under out-of-plane bending. I: Experimental research and finite element modelling. Engineering Structures. 2015;98:230-40.
[10] Gil B, Bijlaard FSK, Bayo E. T-stub behavior under out-of-plane bending. II: Parametric study and analytical characterization. Engineering Structures. 2015;98:241-50.
[11] Gil B, Goñi R, Bayo E. Initial stiffness and strength characterization of minor axis T-stub under out-of-plane bending. Journal of Constructional Steel Research.140:208-21.
[12] Ahmad M, G.Driver R, Callele L, Dowswell B. Design of steel wide-flange members for torsion applied through one flange. Journal of Constructional Steel Research. 2018;141:50-62.
[13] CEN. Eurocode 3 : Design of Steel Structures. Part 1.1: General Rules and Rules for Buildings (EN 1993-1-1:2005): CEN; 2005.
[14] ABAQUS/CAE. 6.8 ed: Hibbit, Karlsson & Sorensen Inc.; 2008.

[15] CEN. ISO 6892-1:2016. Metallic materials. Tensile testing. . Part 1: Method of test at room temperature: CEN; 2016.
[16] CEN. Eurocode 3 : Design of Steel Structures. Part 1.8: Design of Joints (EN 1993-1-8:2005): CEN; 2005.
[17] Lam D, Fu F. Modelling of Semi-rigid Composite Beam-Column Connections with Precast Hollow Core Slabs. Advances in Steel Structures. 2005;1:787-92.
[18] Gil B, Goñi R, Bayo E. Experimental and numerical validation of a new design for three-dimensional semi-rigid composite joint under general loads. Engineering Structures. 2013;48:55-69.
[19] Gil B, Goñi R. T-stub behaviour under out-of-plane bending. I: Experimental research and finite element modelling. Engineering Structures. 2015;98:230-40.
[20] Hughes AF, Iles DC, Malik AS. Design of steel beams in torsion. Berkshire, United Kingdom: SCI (Steel Construction Institute); 2011.